Published in final edited form as:

Magn Reson Imaging. 2017 June ; 39: 194–199. doi:10.1016/j.mri.2017.02.009.

Direct Magnitude and Phase Imaging of Myelin Using Ultrashort Echo Time (UTE) Pulse Sequences: a Feasibility Study

Qun He[1,2], **Yajun Ma**[1], **Shujuan Fan**[1], **Hongda Shao**[1], **Vipul Sheth**[1], **Graeme M Bydder**[1], and **Jiang Du**[1]

[1]Department of Radiology, University of California, San Diego

[2]Ningbo Jansen NMR Technology Co., Ltd., Cixi, Zhejiang Province, China

Abstract

In this paper, we aimed to investigate the feasibility of direct visualization of myelin, including myelin lipid and myelin basic protein (MBP), using two-dimensional ultrashort echo time (2D UTE) sequences and utilize phase information as a contrast mechanism in phantoms and in volunteers. The standard UTE sequence was used to detect both myelin and long T2 signal. An adiabatic inversion recovery UTE (IR-UTE) sequence was used to selectively detect myelin by suppressing signal from long T2 water protons. Magnitude and phase imagingand T2* were investigated on myelin lipid and MBP in the forms of lyophilized powders as well as paste-like phantoms with the powder mixed with D_2O, and rubber phantoms as well as healthy volunteers. Contrast to noise ratio (CNR) between white and gray matter was measured. Both magnitude and phase images were generated for myelin and rubber phantoms as well white matter in vivo using the IR-UTE sequence. T2* values of ~300 μs were comparable for myelin paste phantoms and the short T2* component in white matter of the brain in vivo. Mean CNR between white and gray matter in IR-UTE imaging was increased from -7.3 for the magnitude images to 57.4 for the phase images. The preliminary results suggest that the IR-UTEsequence allows simultaneous magnitude and phase imaging of myelin in vitro and in vivo.

Keywords

white matter; myelin; UTE; IR-UTE; T2*; magnitude; phase

Introduction

The myelin sheath is a multi-lamellar membrane that insulates the axon from electrical activity and functions to increase the rate of action potential transmission (1). The myelin sheath has a characteristic ultrastructure consisting of alternating layers of protein and lipid (2). Myelin is a relatively dehydrated structure, with a water content of approximately 40% in situ (3). The low water content of white matter (72%) as compared to gray matter (82%) is largely due to the high myelin content of white matter (4). Isolated myelin is largely composed of macromolecules (70-85% lipid and 15-30% protein) (5).

Corresponding Address: Jiang Du, Ph.D. jiangdu@ucsd.edu University of California, San Diego, Department of Radiology, 200 West Arbor Drive, San Diego, CA 92103-8756, Phone (619) 543-3512.

Abnormalities in myelination are seen in a number of diseases, including multiple sclerosis, which is the most common demyelinating disease of the central nervous system (6). Magnetic resonance (MR) imaging is the standard imaging modality for the brain and conventional sequences are very sensitive to white matter diseases, but specificity is limited with a broad range of pathologies that lead to similar signal intensity alterations, including inflammation, gliosis, edema, axonal loss, and demyelination (6,7).

This lack of specificity is, in part, due to the inability of conventional sequences to directly image the majority of myelin components, notably the macromolecules (lipids and proteins). Conventional MR imaging techniques use longer echo times, which only capture signals originating from highly mobile protons found in water molecules (with T2 times greater than 10 ms) (8). Hydrogen protons that are located in the macromolecules are less mobile and demonstrate much shorter T2 times (ranging from tens of microseconds up to one millisecond). Therefore, the signal from these protons has decayed to near zero long before conventional data acquisition (9,10). A number of indirect approaches for imaging of the short T2 components of myelin have been proposed in the literature, including magnetization transfer imaging and multi-exponential T2 imaging (8).

Direct MR imaging of both long T2 white matter (WM_L) and short T2 component (i.e., myelin) has been performed using ultrashort echo time (UTE) techniques on nuclear magnetic resonance (NMR) spectrometers (9,10). We have recently shown that high-contrast, selective imaging of the short T2 component of white matter can be achieved on a clinical 3T scanner using an adiabatic inversion recovery (IR) preparation pulse together with a dual echo UTE acquisition beginning with echo time as short as 8 μs (11).

In recent years, MR phase images have been shown to offer a new means of contrast for neuroimaging applications. Importantly, phase information requires no additional scanning time and is an inherent part of the MR image. Using gradient-echo phase images, contrast-to-noise ratios between gray and white matter can be improved 10-100 times over conventional magnitude images and in some instances can reveal structures that are not otherwise visible (12,13). To date, evaluation of phase information using UTE sequences has been limited (14,15).

The purpose of this study is to demonstrate the feasibility of direct visualization of the macromolecular component of myelin using two-dimensional (2D) UTE sequences on a clinical 3T scanner and to utilize phase information as a potential contrast mechanism in phantom and in vivo studies.

Methods

Pulse Sequence

A 2D adiabatic inversion recovery prepared dual echo UTE (2D IR-UTE) sequence as shown in Figure 1 was implemented on a 3T Signa Twin Speed clinical, whole-body scanner (GE Healthcare Technologies, Milwaukee, WI)which had a maximum gradient performance of 40 mT/m and 150 mT/m/ms. The basic 2D UTE sequence employs a half-pulse radiofrequency (RF) excitation (pulse duration = 472 μs, spectral bandwidth = 2.7 kHz) with

the peak RF power deposited during the ramp down part of the slice selection gradient (16). A minimal nominal TE of 8 μs can be achieved between the end of the RF excitation and the beginning of the free induction decay (FID) data acquisition by combining 2D radial ramp sampling, variable rate selective excitation (VERSE) and fast transmit/receive (T/R) switching. The 2D UTE sequence requires the summation of two sets of data acquired with the slice selection gradient in positive and negative polarities, respectively, in order to achieve slice-selective excitation. An adiabatic Silver-Hoult inversion pulse (duration = 8.64 ms, spectral bandwidth = 1.5 kHz) is used to invert the longitudinal magnetization of WM_L. The longitudinal magnetization of myelin is not inverted but largely saturated by the adiabatic inversion pulse, which has a duration much longer than the T2* of myelin protons (in the order of a few hundred microseconds). The 2D UTE data acquisition starts after a delay of time to the null (TI), when the inverted longitudinal magnetization of WM_Lapproaches the null point. The longitudinal magnetization of myelin protons recovered during TI is subsequently excited by the short half-pulse, and detected by the 2D radial ramp sampling, thus allowing direct phase imaging of myelin protons.In dual echo IR-UTE imaging, the 2^{nd} echo contains signal from gray matter, with near zero signal from WM_L (being inverted and nulled) and myelin (due to its ultrashort T2* and fast signal decay). Subtraction of the 2^{nd} echo from the FID provides selective imaging of myelin. The dual-echo IR-UTE imaging was applied to in vivo studies while only single echo IR-UTE imaging was applied to phantom studies (details below).

Phantom Studies

Two sets of phantoms were designed for this study. First, myelin phantoms were prepared for validation of direct phase imaging of myelin using UTE sequences. Second, a rubber phantom, which has similar T2* as that of myelin protons, was prepared to test the feasibility of efficient long T2 suppression and selective phase imaging of rubber. This is essential for selective phase imaging of myelin in an in vivo setting.

Four myelin phantoms were prepared for this study. The first one was a biologically derived bovine myelin lipid powder phantom (type-I bovine brain extract obtained from Signa-Aldrich Corp, St. Louis, MO), which is an organophilic extract of predominantly myelin-related brain lipids. The second phantom was bovine brain extract powder combined with deionized $D_2O$to form a suspension. The third phantom was 90% purified (SDS-PAGE) bovine myelin basic protein (MBP) powder obtained from Sigma-Aldrich Corp. The fourth phantom was synthetic myelin lipid formulated to approximate the non-protein portion of biological myelin including cholesterol, galactocerebroside, phosphatidylcholine and sphingomyelin (all lipids from Sigma-Aldrich Corp). The powder was mixed with deionized D_2O to form a suspension. The phantoms were imaged with the basic 2D UTE sequence as well as the IR-UTE sequence. The following imaging parameters were used: FOV = 4 cm, bandwidth = 62.5 kHz, flip angle = 10°, TR = 100 ms, reconstruction matrix = 128×128, number of projections = 403, a series of TEs (TEs = 8 μs, 0.1, 0.2, 0.3, 0.4, 0.5, 0.8, 1.5 ms), scan time = 40 seconds per acquisition. The TI for use with the IR-UTE sequence was determined for each tissue phantom from measurement of the T_1 of the longer T_2 component (when it was present) using the clinical IR-FSE sequence. A 1-inch solenoid coil was used

for signal excitation and reception. Magnitude and phase images were generated for each UTE acquisition. The T2* of myelin protons was fitted with a single-component model.

The rubber phantom was prepared by immersing a pink rubber (Paper Mate, Oak Brook, IL) into 1% agarose gel. The agarose gel was doped with gadolinium so that it had a T1 of around 800 ms, approximating that of long T2 white matter in the human brain. We employed this phantom to test whether agarose gel could be efficiently suppressed by the IR-UTE sequence, thus providing selective phase imaging of the rubber eraser which has a T2* similar to that of myelin protons. The phantom was imaged with the 2D IR-UTE sequence. The following imaging parameters were used: FOV = 8 cm, bandwidth = 125 kHz, flip angle = 60°, TR = 1000 ms, TI = 280 ms, reconstruction matrix = 256×256, number of projections = 255, a series of TEs (TEs = 8 μs, 0.1, 0.2, 0.3, 0.4, 0.6, 0.8, 1, 1.2, 1.6, 2, 2.5, 3, 4, 5, 6, 7, 8 ms), scan time = 3 minutes per acquisition. A birdcage coil was used for signal excitation and reception. Magnitude and phase images were generated for each UTE acquisition. The T2* of the rubber eraser was fitted with a single-component model.

Human Studies

In total five volunteers were recruited for this technical feasibility study. Written informed consent approved by the Institutional Review Board (IRB)was obtained prior to the participation of each subject. A clinical IR-FSE sequence was used to measure the T1 of WM_L. The 2D IR-UTE sequence was used for direct magnitude and phase imaging of myelin with the following parameters: FOV = 24 cm, slice thickness = 5 mm, bandwidth = 250 kHz, flip angle = 70°, TR = 1500 ms, TI ~ 420 ms (slightly adjusted based on T1 variation in long T2 white matter), four dual echo acquisitions (TE = 8 μs/4.4 ms; 0.2/4.4 ms, 0.6/4.4 ms, 1.5/4.4 ms), projections=131, reconstruction matrix=256×256, scan time=6.5 min per acquisition. An 8-channel head coil was used for signal reception. Magnitude images were generated via sum-of-square combination of the images from each coil. Phase images was reconstructed using an adaptive implementation of the spatial matched filter (17).Contrast to noise ratio (CNR) between white and gray matter was measuredin IR-UTE magnitude and phase images with a TE of 8 μs. CNR was calculated as the signal difference between white and gray matter over the standard deviation of the background noise.

Results

Figure 2 shows selected UTE images of the bovine brain extract powder phantom. Myelin signal dropped to near zero at 0.4 ms. Single-component fitting of the UTE images suggests a short T2* of 167 ± 7 μs. The IR-UTE images show nearly the same short T2* of 163 ± 6 μs. Phase images were generated with high contrast, demonstrating the feasibility of direct phase imaging of myelin protons using UTE sequences on a clinical 3T scanner.

Figure 3 shows both the magnitude and phase images of the myelin MBP powder phantom. The bright signal from the MBP powder phantom demonstrates that protons in MBP are detectable with UTE sequences on a clinical 3T scanner. Obvious image blurring was observed likely due to the extremely short T2*s of MBP protons. Indeed, an excellent

single-exponential fitting was achieved on the UTE images of MBP powder, and an ultrashort T2* of 172 ± 12 μs was demonstrated. A similar T2* of 160 ± 5 μs was demonstrated by fitting the corresponding IR-UTE images.

Figure 4 shows selected magnitude and phase images of the bovine brain lipid and MBP powders mixed with D_2O, and the corresponding exponential fitting of IR-UTE images. A short T2* of 310 ± 21 μs was demonstrated for the myelin lipid paste. A similar short T2* of 299 ± 14 μs was demonstrated for the MBP paste. The paste phantoms have longer T2* than the powder phantoms likely due to reduced susceptibility when the powders were mixed with D_2O to form suspensions.

Figure 5 shows both UTE and IR-UTE images of the rubber phantom. Excellent suppression of the agarose gel and selective magnitude and phase imaging of the rubber were achieved simultaneously using the IR-UTE technique. The rubber signal showed a single-component decay behavior with a short T2* of 321 ± 6 μs, which is very close to the T2* of protons in myelin lipid and myelin basic protein, suggesting thatthe contrast generated with the rubber phantom can potentially be applied to myelin imaging in vivo.

Figure 6 shows dual echo IR-UTE imaging of the brain of a 28-year-old healthy volunteer. The long T2 white matter is efficiently suppressed as evidenced by the near zero signal in the second echo with a TE of 4.4 ms. The short T2 component shows a moderate signal but limited contrast in the 1st echo with a TE of 8 μs, and near zero signal at a TE of 4.4 ms, consistent with imaging of myelin. Signal from residual gray matter is highlighted in the second echo. Subtraction of the 2nd image from the 1st one provided high contrast imaging of myelin. The short T2* component has a T2* of 336 ± 28 μs, which is comparable to that of myelin protons in D_2O suspension, further suggesting that myelin being imaged with the 2D IR-UTE sequence. Also shown is IR-UTE phase imaging. High phase contrast was generated for myelin after efficient suppression of long T2 white matter components. Similar findings were achieved for all five volunteers, demonstrating the consistency of our 2D IR-UTE sequences for direct magnitude and phase imaging of myelin in vivo.Mean CNR between white and gray matter in IR-UTE imaging was increased from -7.3 for the magnitude images to 57.4 for the phase images.

Discussion

Phase images of the brain are of interest since they demonstrate improved contrast compared with magnitude images (12,18,19). However, to date, almost all the studies have employed long echo times (~40 ms). Although this approach allows for evaluation of the gray-white matter interface, the signal and contrast are due to mainly mobile water protons. The majority of myelin components, which demonstrate short T2 relaxation times, can only be visualized using UTE techniques. Only one prior study investigated phase contrast imaging of the brain using an off-resonance saturated 3D UTE sequence and reported enhanced phase contrast in the midbrain (15). The results of our study show that phase images generated using UTE techniques can provide direct, high contrast imaging of myelin lipid and myelin basic protein.

Myelinated white matter demonstrates several distinct compartments, including the axonal space, myelin sheath, and the interstitial space, which cause the proton frequency values to vary over a range (20-22). As a whole, the myelin sheath has shorter T1, T2, and T2* relaxation times compared with the other compartments (23-27). However, the myelin sheath also has distinct proton pools, including the protons in myelin-associated water (T2* ~3-10 ms) (28,29) and macromolecular protons (T2* ~tens μs – 1 ms) (8-11). Our results show that selective high-contrast phase imaging can be performed on the myelin macromolecular component based on T2 separation (using the IR-UTE technique) and that quantification can be performed on this compartment.

The phase information derived from the IR-UTE approach is likely different from that derived from UTE acquisition with off-resonance saturation (15,30). In the latter approach, 360° adiabatic pulses were applied ±1.2 kHz to partially saturation the broad line short-T2 resonance (15). The subtraction of UTE images without and with off-resonance saturation provides enhanced phase contrast for the short T2 components. The authors suggest that the signal sources might include bounded protons or restricted water pools although no direct evidence was provided (e.g., no T2* values measured). The IR-UTE approach is likely more selective in imaging the very short T2 components since the longitudinal magnetizations of the longer T2 components are inverted and nulled by the adiabatic inversion pulse. The short T2 components have T2*s of ~300 μs, approaching that of myelin protons, suggesting that the signal sources are mainly myelin lipid and myelin basic protein. Signals from other macromolecules or short T2 connective structures may also contribute to the IR-UTE image. More research is needed to understand the mechanism and signal contribution to IR-UTE magnitude and phase images.

There are different approaches for combining phase images acquired using phased array coils. An adaptive phase alignment technique was proposed to combine the individual coil outputs prior to image formation (31). Later an adaptive implementation of the spatial matched filter employing locally relevant array correlation statistics and eigen-analysis was used to provide a near-optimal reconstruction of phased array MR images without a priori knowledge of the individual coil field maps or noise correlation structure (17). More recently, Liu et al. employed the low-pass filtered phase difference (i.e. coil phase) to calculate the coil-phase-removed phase maps and the magnitude maps from different coils, and then reconverted them into complex data and averaged (15). Phase from the averaged complex data was unwrapped using the Laplacian-based phase unwrapping algorithm (32). Here we choose the adaptive method described by Walsh et al. (17). Quantitative comparison between these different approaches remain to be investigated.

Direct high-contrast visualization and the ability for quantification of the macromolecular component of myelin have a number of potential applications. This technique may improve the sensitivity and specificity of diagnosis and therapeutic monitoring of diseases that specifically target myelin. For instance, in multiple sclerosis plaques, biochemical studies have shown that there is a decrease in total lipid as well as myelin basic protein as a result of myelin loss (33). Many drugs have been designed to enhance re-myelination (34), however, the lack of a robust biomarker for re-myelination has remained problematic. Indirect assessment of myelin by magnetization transfer (MT) has shown promise in the assessment

of regeneration and stabilization of myelin damage (35). The magnitude and phase images acquired with the IR-UTE sequences may be useful for more direct evaluation of demyelination and re-myelination.

While our study demonstrates the technical feasibility of phase contrast images of the components of myelin, a number of limitations exist. First, the IR-UTE approach may not perfectly suppress all long T2 water within white matter, including myelin-associated water, somewhat reducing the selectively. However, our earlier studies have shown that a single adiabatic inversion pulse can be used to simultaneously suppress tissues with different T1 values. Specifically we have shown that both muscle and fat, which have different T1 values, can be suppressed by more than 90% with a single inversion pulse when imaging the short T2 components of cortical bone (16). Therefore, although water may contribute to some signal using the IR-UTE technique, the significant majority of the signal is from the macromolecules. Second, we are generating phase images using UTE techniques and it may be argued that phase accumulation occurs to a greater degree at longer TEs. However, previous studies have shown that unlike conventional sequences which accumulate phase predominantly during the time to echo, UTE sequences with radial readout trajectories accumulate phase most during the RF excitation and radial readout (14,15). Third, the advantages and disadvantages of direct myelin magnitude and phase imaging with IR-UTE techniques over indirect myelin imaging with MT techniques remain to be investigated. Fourth, the relation between myelin phase and myelin content was not investigated. Future studies will be conducted to investigate the phase change in phantoms with different myelin-D_2O ratios, and in cadaveric MS specimens. Fifth, applications of simultaneous magnitude and phase imaging of myelin in MS patients, especially these patients under therapeutic treatment would be full of interest and remain to be investigated.

In conclusion, we demonstrate that UTE sequences can be used to detect the rapidly decaying signal from the macromolecular components of myelin and that high-contrast phase images can be generated. Furthermore, these morphological and quantitative techniques can be readily translated for in vivo imaging.

Acknowledgments

This study was supported by the National Institutes of Health (R01NS092650).

References

1. Raine, CS. Morphology of myelin and myelination. In: Morell, P., editor. Myelin. Plenum; New York: 1984. p. 1-41.
2. Morell, P., Quarles, RH. The Myelin Sheath. In: Siegel, GJ.Agranoff, BW., Albers, RW., editors. Basic Neurochemistry: Molecular, Cellular and Medical Aspects. 6th. Lippincott-Raven; Philadelphia: 1999.
3. Finean JB. Electron microscope and x-ray diffraction studies of the effects of dehydration on the structure of nerve myelin. II. Optic nerve. J Biophys Biochem Cytol. 1960; 8:31–37. [PubMed: 13699578]
4. Norton, WT., Cammer, W. Isolation and Characterization of Myelin. In: Morell, P., editor. Myelin. Plenum; New York: 1984. p. 155

5. Morell, P., Quarles, RH. Characteristic Composition of Myelin. In: Siegel, GJ.Agranoff, BW., Albers, RW., editors. Basic Neurochemistry: Molecular, Cellular and Medical Aspects. 6th. Lippincott-Raven; Philadelphia: 1999.
6. Filippi M, Rocca MA. MR imaging of multiple sclerosis. Radiology. 2011; 259:659–681. [PubMed: 21602503]
7. Bruck W, Bitsch A, Kolenda H, Bruck Y, Stiefel M, Lassmann H. Inflammatory central nervous system demyelination: correlation of magnetic resonance imaging findings with lesion pathology. Ann Neurol. 1997; 42:783–793. [PubMed: 9392578]
8. Alonso-Ortiz E, Levesque IR, Pike GB. MRI-based myelin water imaging: A technical review. Magn Reson Med. 2015; 73:70–81. [PubMed: 24604728]
9. Horch RA, Gore JC, Does MD. Origins of the ultrashort-T2 1H NMR signals in myelinated nerve: a direct measure of myelin content? Magn Reson Med. 2011; 66:24–31. [PubMed: 21574183]
10. Wilhelm MJ, Ong HH, Wehrli SL, Li C, Tsai PH, Hackney DB, Wehrli FW. Direct magnetic resonance detection of myelin and prospects for quantitative imaging of myelin density. Proc Natl Acad Sci USA. 2012; 109:9605–9610. [PubMed: 22628562]
11. Du J, Ma GL, Li SH, Carl M, Szeverenyi NM, Vanden Berg S, Corey-Bloom J, Bydder GM. Ultrashort echo time (UTE) magnetic resonance imaging of the short T2 components in white matter of the brain using a clinical 3T scanner. Neuroimage. 2013; 87:32–41. [PubMed: 24188809]
12. Duyn JH, van Gelderen P, Li TQ, de Zwart JA, Koretsky AP, Fukunaga M. High-field MRI of brain cortical substructure based on signal phase. Proc Natl Acad Sci USA. 2007; 104:11796–11801. [PubMed: 17586684]
13. Rauscher A, Sedlacik J, Barth M, Mentzel HJ, Reichenbach JR. Magnetic susceptibility-weighted MR phase imaging of the human brain. AJNR Am J Neuroradiol. 2005; 26:736–742. [PubMed: 15814914]
14. Carl M, Chiang JTA. Investigations of the Origin of Phase Differences Seen with Ultrashort TE Imaging of Short T2 Meniscal Tissue. Magn Reson Med. 2012; 67:991–1003. [PubMed: 21898582]
15. Liu, CL., Li, W., Larson, P. Off-resonance saturation enhanced phase contrast of the brain at ultra-short TE. Proceedings of the 21th Annual Meeting of ISMRM; Salt Lake City, USA. 2013; p. 766
16. Du J, Carl M, Bydder M, Takahashi A, Chung CB, Bydder GM. Qualitative quantitative ultrashort echo time (UTE) imaging of cortical bone. J Magn Reson. 2010; 207:304–311. [PubMed: 20980179]
17. Walsh DO, Gmitro AF, Marcellin MW. Adaptive Reconstruction of Phased Array MR Imagery. Magn Reson Med. 2000; 43:682–690. [PubMed: 10800033]
18. Lee J, Hirano Y, Fukunaga M, Silva AC, Duyn JH. On the contribution of deoxy-hemoglobin to MRI gray-white matter phase contrast at high field. Neuroimage. 2010; 49:193–198. [PubMed: 19619663]
19. Wu B, Li W, Avram AV, Gho SM, Liu C. Fast and tissue-optimized mapping of magnetic susceptibility and T2* with multi-echo and multi-shot spirals. Neuroimage. 2012; 59:297–305. [PubMed: 21784162]
20. Chen WC, Foxley S, Miller KL. Detecting microstructural properties of white matter based on compartmentalization of magnetic susceptibility. Neuroimage. 2013; 70:1–9. [PubMed: 23268785]
21. Sukstanskii AL, Yablonskiy DA. On the role of neuronal magnetic susceptibility and structure symmetry on gradient echo MR signal formation. Magn Reson Med. 2014; 71:345–353. [PubMed: 23382087]
22. Wharton S, Bowtell R. Fiber orientation-dependent white matter contrast in gradient echo MRI. Proc Natl Acad Sci USA. 2012; 109:18559–18564. [PubMed: 23091011]
23. Andrews T, Lancaster JL, Dodd SJ, Contreras-Sesvold C, Fox PT. Testing the three-pool white matter model adapted for use with T2 relaxometry. Magn Reson Med. 2005; 54:449–454. [PubMed: 16032666]
24. Deoni SC, Matthews L, Kolind SH. One component? Two components? Three? The effect of including a nonexchanging “free” water component in multicomponent driven equilibrium single pulse observation of T1 and T2. Magn Reson Med. 2013; 70:147–154. [PubMed: 22915316]

25. Dortch RD, Harkins KD, Juttukonda MR, Gore JC, Does MD. Characterizing inter-compartmental water exchange in myelinated tissue using relaxation exchange spectroscopy. Magn Reson Med. 2013; 70:1450–1459. [PubMed: 23233414]

26. Sati P, van Gelderen P, Silva AC, Reich DS, Merkle H, de Zwart JA, Duyn JH. Micro-compartment specific T2* relaxation in the brain. Neuroimage. 2013; 77:268–278. [PubMed: 23528924]

27. Du J, Sheth V, Qun H, Carl M, Chen J, Corey-Bloom J, Bydder GM. Measurement of T1 of the ultrashort T2* components in white matter of the brain at 3T. PLoS ONE. 2014; 9(8):e103296. [PubMed: 25093859]

28. Hwang D, Kim DH, Du YP. In vivo multi-slice mapping of myelin water content using T-2* decay. Neuroimage. 2010; 52:198–204. [PubMed: 20398770]

29. Oh SH, Bilello M, Schindler M, Markowitz CE, Detre JA, Lee J. Direct visualization of short transverse relaxation time component (ViSTa). Neuroimage. 2013; 83:485–492. [PubMed: 23796545]

30. Du J, Takahashi AM, Bydder M, Chung CB, Bydder GM. Ultrashort TE imaging with off-resonance saturation contrast (UTEOSC). Magn Reson Med. 2009; 62(2):527–31. [PubMed: 19449436]

31. Debbins JP, Felmlee JP, Riederer SJ. Phase alignment of multiple surface coil data for reduced bandwidth and reconstruction requirements in volumetric MRI applications. Magn Reson Med. 1997; 38:1003–1011. [PubMed: 9402202]

32. Li W, Wu B, Liu C. Quantitative susceptibility mapping of human brain reflects spatial variation in tissue composition. Neuroimage. 2011; 55(4):1645–56. [PubMed: 21224002]

33. Wood DD, Moscarello MA. Is the Myelin Membrane Abnormal in Multiple-Sclerosis. Journal of Membrane Biology. 1984; 79:195–201. [PubMed: 6088773]

34. Kremer D, Kury P, Dutta R. Promoting remyelination in multiple sclerosis: Current drugs and future prospects. Multiple Sclerosis Journal. 2015; 21:541–549. [PubMed: 25623245]

35. van der Knaap, MS., Valk, J. Magnetic resonance of myelination and myelin disorders. Heilmann, U., Mennecke-Buhler, D., editors. Springer Berlin; 2005. p. 1-19.

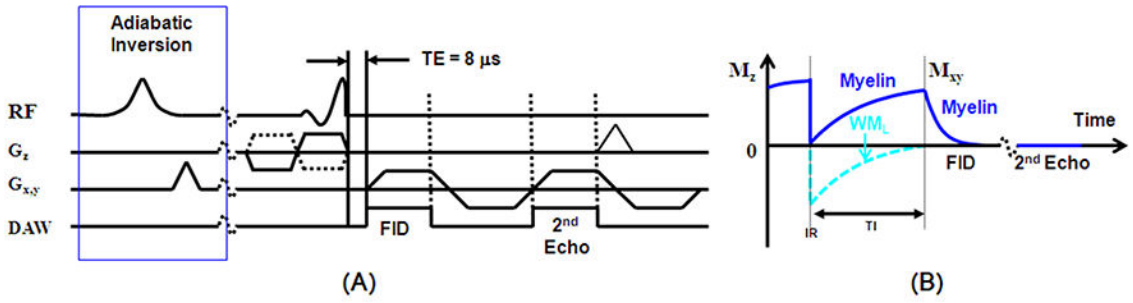

Figure 1.

Pulse sequence for 2D UTE imaging using half pulse excitation and radial ramp sampling with a minimal nominal TE of 8 μs (A). An adiabatic IR preparation pulse together with dual echo acquisition was used to create short T2 contrast (B). The adiabatic IR pulse provides robust inversion of the longitudinal magnetizations of the long T2 components in white matter (WM_L). Myelin has ultrashort T2* and experience significant transverse relaxation during the long adiabatic inversion process, and is not inverted but saturated. UTE acquisition starts when the inverted longitudinal magnetization of WM_L reaches the null point, leaving signals from myelin to be detected by the FID acquisition. The 2nd echo contains signal from gray matter, with near zero signal from myelin due to its ultrashort T2*. Subtraction of the 2nd echo from the FID provides selective imaging of myelin.

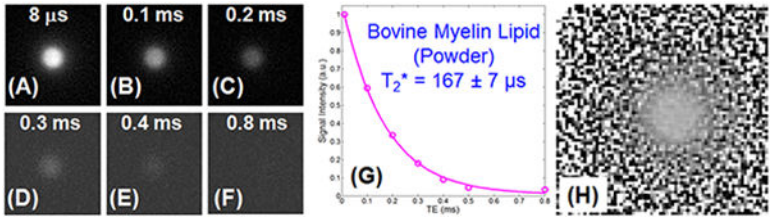

Figure 2.

2D non-slice selective UTE imaging of a bovine brain extract powder phantom with TEs of 8 μs (A), 0.1 ms (B), 0.2 ms (C), 0.3 ms (D), 0.4 ms (E) and 0.8 ms (F), as well as single-component exponential signal decay fitting of UTE images which shows a short T2* of 167±7 μs (G), and UTE phase imaging (H). Phase contrast can be generated for myelin lipid protons in bovine brain extract power despite of its extremely short T2* relaxation time.

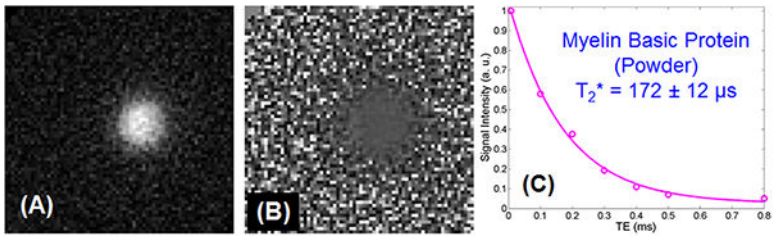

Figure 3.

Magnitude (A) and phase (B) imaging of the myelin MBP powder phantom, as well as single-exponential decay fitting of UTE images of myelin basic protein (MBP) powder which shows a short T2* of 172 ± 12 μs (C).

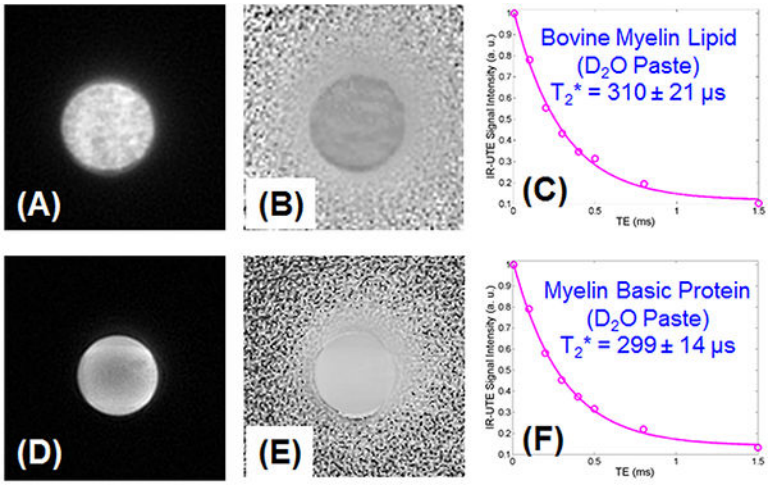

Figure 4.

Magnitude (A) and phase (B) imaging of the bovine myelin lipid powder in D_2O suspension, and magnitude (C) and phase (D) imaging of the MBP powder in D_2O suspension, as well as exponential fitting of IR-UTE images which shows a short T2* of 310±21 μs for the myelin lipid paste phantom, and a short T2* of 299±14 μs for the MBP paste phantom.

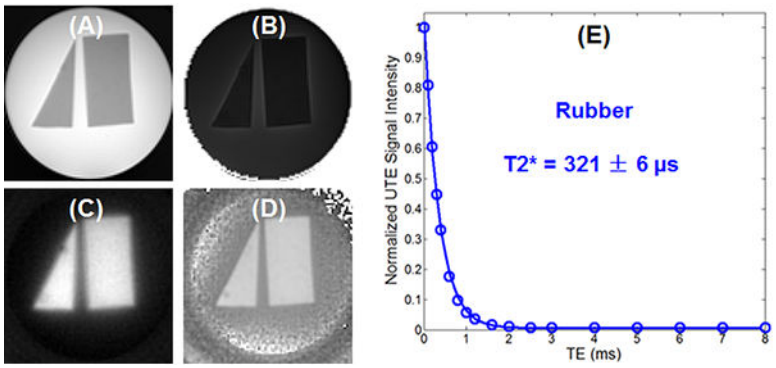

Figure 5.

shows both UTE and IR-UTE images of the rubber phantom. Excellent suppression of the agarose gel and selective magnitude and phase imaging of the rubber were achieved simultaneously using the IR-UTE technique. The rubber signal showed a single-component decay behavior with a short T2* of 321 ± 6 μs, which is slightly longer than T2* of protons in myelin lipid and myelin basic protein.

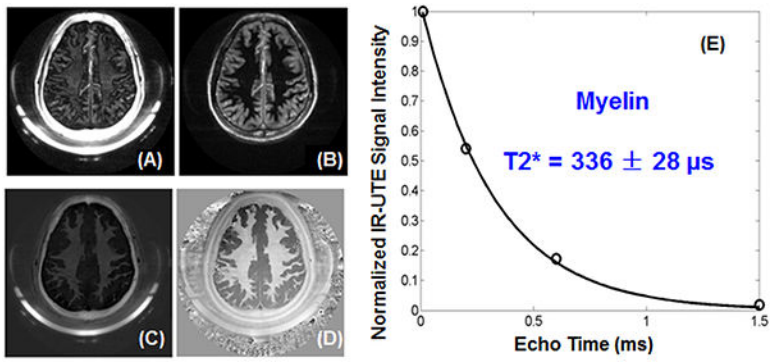

Figure 6.

IR-UTE imaging of the brain of a 38-year-old male volunteer with a TE of 8 µs (A) and 4.4 ms (B). Subtraction of the second echo from the 1st echo provides high contrast for myelin (C). Adaptive phase reconstruction of the phased array images provides high phase contrast (D). The weak signal from the white matter shows a fast decay with a short T2* of 336 ± 28 µs (E), suggesting WM_L being suppressed and myelin being detected.